

# Reversal of global atmospheric ethane and propane trends largely due to US oil and natural gas production

Detlev Helmig<sup>1\*</sup>, Samuel Rossabi<sup>1</sup>, Jacques Hueber<sup>1</sup>, Pieter Tans<sup>2</sup>, Stephen A. Montzka<sup>2</sup>, Ken Masarie<sup>2</sup>, Kirk Thoning<sup>2</sup>, Christian Plass-Duelmer<sup>3</sup>, Anja Claude<sup>3</sup>, Lucy J. Carpenter<sup>4</sup>, Alastair C. Lewis<sup>5</sup>, Shalini Punjabi<sup>4</sup>, Stefan Reimann<sup>6</sup>, Martin K. Vollmer<sup>6</sup>, Rainer Steinbrecher<sup>7</sup>, James W. Hannigan<sup>8</sup>, Louisa K. Emmons<sup>8</sup>, Emmanuel Mahieu<sup>9</sup>, Bruno Franco<sup>9</sup>, Dan Smale<sup>10</sup> and Andrea Pozzer<sup>11</sup>

**Non-methane hydrocarbons such as ethane are important precursors to tropospheric ozone and aerosols. Using data from a global surface network and atmospheric column observations we show that the steady decline in the ethane mole fraction that began in the 1970s<sup>1–3</sup> halted between 2005 and 2010 in most of the Northern Hemisphere and has since reversed. We calculate a yearly increase in ethane emissions in the Northern Hemisphere of  $0.42 (\pm 0.19) \text{ Tg yr}^{-1}$  between mid-2009 and mid-2014. The largest increases in ethane and the shorter-lived propane are seen over the central and eastern USA, with a spatial distribution that suggests North American oil and natural gas development as the primary source of increasing emissions. By including other co-emitted oil and natural gas non-methane hydrocarbons, we estimate a Northern Hemisphere total non-methane hydrocarbon yearly emission increase of  $1.2 (\pm 0.8) \text{ Tg yr}^{-1}$ . Atmospheric chemical transport modelling suggests that these emissions could augment summertime mean surface ozone by several nanomoles per mole near oil and natural gas production regions. Methane/ethane oil and natural gas emission ratios could suggest a significant increase in associated methane emissions; however, this increase is inconsistent with observed leak rates in production regions and changes in methane's global isotopic ratio.**

Oxidation of atmospheric non-methane hydrocarbons (NMHCs) contributes to production of surface ozone and secondary aerosol, both of which impact air quality and climate. NMHCs are emitted into the atmosphere from a variety of biogenic and anthropogenic sources. Ethane is the longest-lived and most abundant NMHC, found typically at  $\sim 0.4\text{--}2.5 \text{ nmol mol}^{-1}$  (ppb) in the background atmosphere. It is released from seepage of fossil carbon deposits, volcanoes, fires, and from human activities, with fossil fuel extraction, distribution leakage, and industrial use being the main sources. Pre-industrial ethane atmospheric mole fractions measured in polar ice cores were  $\sim 400 \text{ pmol mol}^{-1}$  in the

Northern Hemisphere (NH) and  $\sim 100 \text{ pmol mol}^{-1}$  in the Southern Hemisphere (SH), that is between  $\sim 1/4\text{--}1/2$  of current levels<sup>4</sup>. Firn air records<sup>1–3</sup> show that in the early part of the twentieth century NMHCs increased steadily in the global atmosphere. Light alkane NMHCs ( $\text{C}_2\text{--C}_5$ ) reached a maximum that was  $\sim 50\%$  above 1950 levels during 1970–1985. Global atmospheric ethane peaked around 1970. NMHCs have since been steadily declining to mole fractions that are closer to the earliest data in the Greenland firn record (Fig. 1a). These trends are primarily due to stricter air quality emission controls that were first implemented some 50 years ago with the goal to reduce human exposure to NMHCs and surface ozone. The regulations resulted in reduced emissions from sources such as the oil and natural gas (O&NG) industries and automobiles, and a gradual decline of atmospheric NMHCs in urban air in many developed countries and also in the background atmosphere<sup>5–7</sup>.

Ethane and methane are co-emitted from O&NG sources. Ethane observations have been used to attribute anthropogenic methane emission changes<sup>7</sup>. Having the longest NMHC lifetime, of the order of 2 (summer) to 6 (winter) months, ethane is the NMHC observed with the least spatial and short-term variability in background air, making it the best candidate species for studying hemispheric gradients and long-term changes.

We analysed ten years of NMHC data collected at 44 remote global sampling sites from the National Oceanic and Atmospheric Administration (NOAA) Global Greenhouse Gas Reference Network (GGGRN). We also include data from *in situ* monitoring at Summit, Greenland<sup>8</sup>, at Hohenpeissenberg (HPB) in Southern Germany<sup>9</sup>, Jungfraujoch (JFJ) and Rigi, Switzerland, and Cape Verde in the Mid-Atlantic<sup>10</sup>. For propane, we further included results from eight sites within NOAA's GGGRN (Methods).

Atmospheric NMHCs exhibit a dynamic seasonal and latitudinal behaviour. Maxima are seen in late winter, and minima in the summer (Fig. 1b–e). Sources of light NMHCs do not vary much seasonally<sup>11</sup>; seasonal cycles are primarily driven by photochemical loss. Consequently, seasonal cycles exhibit the largest amplitude

<sup>1</sup>Institute of Arctic and Alpine Research, University of Colorado, Boulder, Colorado 80305, USA. <sup>2</sup>Earth Systems Research Laboratory, National Oceanic and Atmospheric Administration, Boulder, Colorado 80305, USA. <sup>3</sup>Deutscher Wetterdienst, 82383 Hohenpeissenberg, Germany. <sup>4</sup>Wolfson Atmospheric Chemistry Laboratories, University of York, York YO10 5DD, UK. <sup>5</sup>National Centre for Atmospheric Science, University of York, York YO10 5DD, UK. <sup>6</sup>Laboratory for Air Pollution and Environmental Technology, Empa, Swiss Federal Laboratories for Materials Science and Technology, 8600 Duebendorf, Switzerland. <sup>7</sup>Karlsruhe Institute for Technology, Campus Alpine, 82467 Garmisch-Partenkirchen, Germany. <sup>8</sup>National Center for Atmospheric Research, Boulder, Colorado 80301, USA. <sup>9</sup>Institute of Astrophysics and Geophysics, University of Liège, 4000 Liège, Belgium. <sup>10</sup>National Institute of Water and Atmospheric Research, Lauder 9352, New Zealand. <sup>11</sup>Max Planck Institute for Chemistry, 55128 Mainz, Germany. \*e-mail: [detlev.helmig@colorado.edu](mailto:detlev.helmig@colorado.edu)

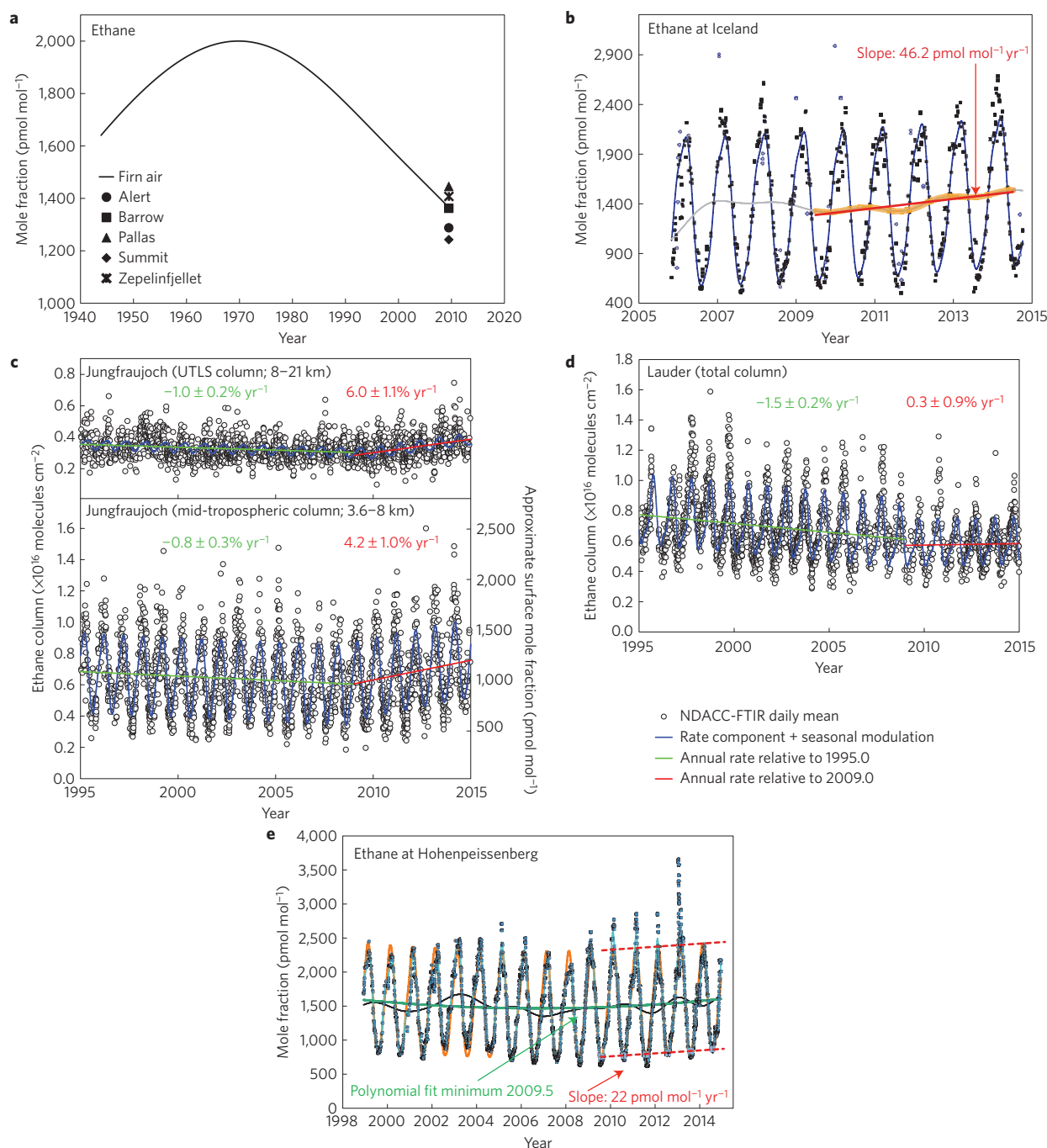


**Figure 1 | Histories of atmospheric ethane.** **a**, Reconstructed 1950–2010 ethane history from firn air sampling at NEEM in Greenland<sup>3</sup> with 2009.5 mean seasonally detrended atmospheric values at five Arctic sites for comparison. Data from ref. 3. **b**, Ten years of NMHC flask network data in south Iceland. Individual flask data, identified outliers (smaller blue points), a smoothed fit, the trend results after removal of harmonic components, and the linear regression fit are shown, with a  $46.2 \text{ pmol mol}^{-1} \text{ yr}^{-1}$  increase from 2009.5 to 2014.5. **c,d**, Ethane upper troposphere and lower stratosphere (UTLS), and mid troposphere FTIR columns showing a trend reversal and increasing rate of change after 2009 at Jungfraujoch, Switzerland (**c**), in contrast to Lauder, New Zealand (**d**). **e**, Monthly running median data from the daily *in situ* record at Hohenpeissenberg, with smoothed, function, and trend fits. A polynomial fit shows a minimum in the second half of 2009; the linear regression to the post 2009.5 trend curves and seasonal maxima and minima show increases of  $22\text{--}23 \text{ pmol mol}^{-1} \text{ yr}^{-1}$ .

near the poles, are small near the Equator (Fig. 2), and are shifted by  $\sim 6$  months in the SH owing to the opposite season. There is also a strong latitudinal gradient of absolute values, with highest abundances observed in the Arctic, steeply declining levels at mid-latitudes, and lower abundance in the SH. These gradients are caused by sources that are dominated by anthropogenic emissions, which are highest in the industrialized mid-northern latitudes,

and the slower transport across the equatorial zone compared with intrahemisphere mixing. Gases with shorter lifetimes, that is, propane, *iso*-butane, and *n*-butane, exhibit more pronounced seasonal and latitudinal gradients (Fig. 2).

Individual site data reveal that for many NH locations the downward trend reported in earlier work has halted and reversed to increasing NMHC levels. As the flask network programme started in

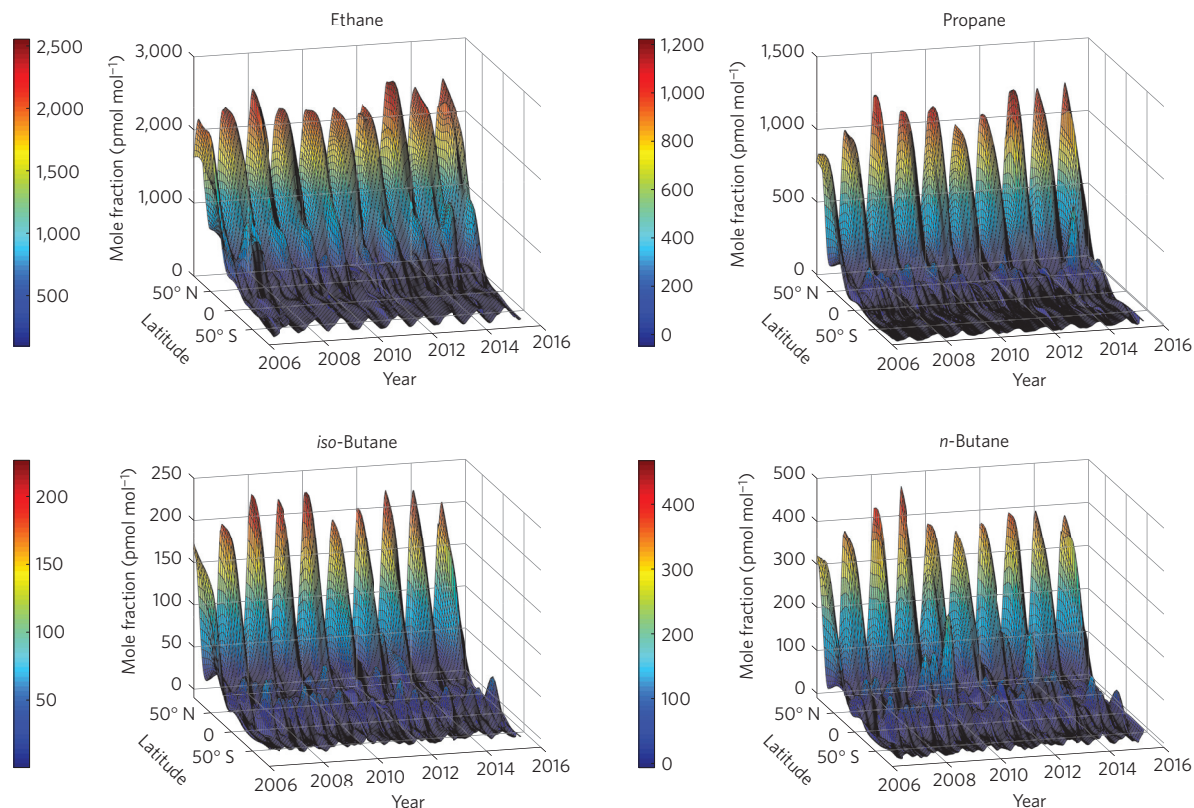


**Figure 2 | Latitudinal distribution of ethane, propane, iso-butane, and n-butane.** These representations of surface mole fractions were generated using weekly data from 37 to 39 global background monitoring sites, altogether some 30,000 data points for each graph. Note that these plots are a representation of latitudinal averages of atmospheric mole fractions; therefore, they do not capture differences between continents at the same latitude. Procedures for data filtering and processing are discussed in the Methods.

2006, data for most sites do not go back far enough for deciphering the exact time of the trend reversal. The second-order polynomial fit through the longest, and most highly time-resolved *in situ* record from HPB has its minimum in 2009 (Fig. 1e), in agreement with the JFJ Fourier transform infrared (FTIR) column observations (Fig. 1c). Focusing on the most recent five years (2009.5–2014.5) we find variable results in the observed rate of change; however, a consistent picture emerges that shows the largest increases at NH sites (Fig. 3). Of 32 NH sites, 9 exhibit ethane growth rates  $>50 \text{ pmol mol}^{-1} \text{ yr}^{-1}$ , and 13 sites exhibit growth rates between 25 and  $50 \text{ pmol mol}^{-1} \text{ yr}^{-1}$  (Supplementary Table 1). Depending on grouping of sites and averaging across regions and calculation method, a mean NH ethane increase rate of  $2.9\text{--}4.7\% \text{ yr}^{-1}$  is calculated (Methods). These rates of change in atmospheric ethane have not been seen at SH sites; most SH sites show only small changes, with poorer regression results. Applying a second-order polynomial fit to the NH trend curves yields positive quadratic coefficients in 22 out of 32 cases, showing that for most cases, ethane trend curves are becoming steeper; that is, rates of change in atmospheric abundance have been increasing at most of the sites during this time window.

This hemispheric difference in ethane trends is further supported by two contrasting records of ethane column observations (that is, the number of molecules integrated between the ground and the top of the atmosphere), one from JFJ (Fig. 1c)<sup>12</sup>, and the other one from Lauder, New Zealand (Fig. 1d). At the 3,580 m elevation of JFJ, these data are a good representation of free tropospheric ethane, reflecting the continental background and long range transport. Whereas there was a slight downward trend in the data for the first 15 years of the record, in agreement with the trends inferred from the firn and HPB data, a reversal is evident after 2009, with a post-2009

rate of increase in the mid-troposphere of  $4.2 \pm 1.0\% \text{ yr}^{-1}$ . The upward trend is evident in both the mid-troposphere and upper troposphere/lower stratosphere partial columns, indicative of the hemispheric nature of the ethane increase. The ethane trend reversal is absent in the SH FTIR column data (Fig. 1d). The difference in trends in the hemispheres is consistent with an increasing NH source.

Notably, ethane rates of change are highest at the central and eastern USA and nearby downwind sites, suggesting that the ethane increase is driven to a large part by emissions from North America. The regional hotspot of increasing NMHC levels can be pinpointed more narrowly from propane observations. Propane, with a lifetime  $\sim 1/4$  of ethane, is a more sensitive indicator for local/regional emissions. Propane data show the greatest increases in the central and eastern USA, and in the downwind North Atlantic region (Fig. 3). In contrast, propane levels have been relatively stable in central Europe, the Pacific region, and the SH. Also, measurements in the western USA do not show propane increases. With the primary synoptic transport direction being west and southwest to east, the spatial analyses of ethane and propane increases point to the central to eastern parts of the USA as the regions where most of the emission increases have occurred.

The O&NG sector is a major source of light NMHC emissions. A surge in O&NG production has occurred in recent years, particularly in the USA, where unconventional oil and natural gas drilling has resulted in estimated 10–20-fold increases in shale O&NG production between 2000 and 2015 ([www.eia.gov](http://www.eia.gov)), making the USA the fastest growing and a leading O&NG producing nation. Ground and airborne observations have consistently shown elevated levels of methane and NMHC as a result of venting, flaring, and leakage. NMHC ambient mole fractions

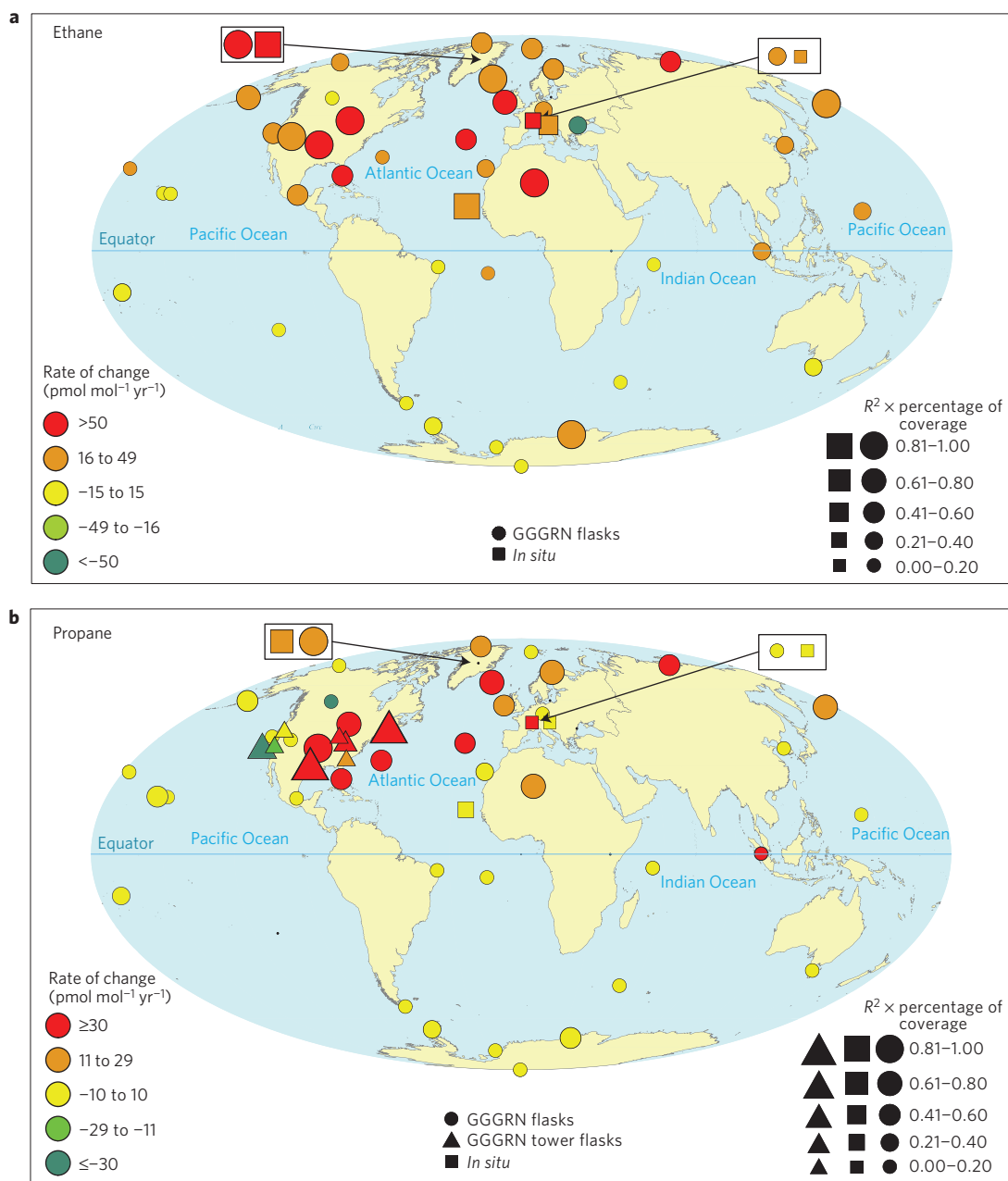


**Figure 3 | Ethane and propane trends at global monitoring sites.** Mole fraction changes are indicated by the colour scale with marker size corresponding to the  $R^2$  of the fit multiplied by the fraction of available site data. Results from overlapping GGGRN flask and *in situ* measurements are shown in black rectangles for Summit and Hohenpeissenberg. **a**, Increasing ethane is observed throughout the NH, with the strongest signal in North America, the North Atlantic, and neighbouring continents. There is no or very little change in ethane at SH sites. **b**, Propane shows a more pronounced region of increasing mole fractions in the eastern USA and at nearby downwind sites. Again, these changes are not seen at the SH sites.

measured in O&NG basins can far exceed (up to >100 times) the regional background and those in urban and other industrial regions, and top-down emission estimates are well above inventory estimates<sup>13–17</sup>. Resulting ozone production from these emissions has led to air quality standard exceedances in the Uintah Basin, Utah, and Upper Green River Basin, Wyoming, O&NG regions<sup>18,19</sup>. Two other regional studies have previously noted upwards trends in ambient NMHC and associated these changes with upwind O&NG activities. An increase from 7% to 13% of the total observed non-methane organic carbon abundance during 2010–2013, and increasing ethane mole fractions were measured in Baltimore, Maryland, downwind of the Marcellus Shale<sup>20</sup>. Similarly, data from southern Texas showed steeply

increasing ethane levels associated with transport from the Eagle Ford Shale<sup>21</sup>.

Applying the JFJ FTIR mid-troposphere column trend value of  $4.2\% \text{yr}^{-1}$  to the NH annual ethane emission estimate of  $9.9 \text{ Tg yr}^{-1}$  (Methods) yields an estimate for an ethane annual emission increase of  $0.42 \pm 0.19 \text{ Tg yr}^{-1}$  (see Methods for all uncertainty range calculations), resulting in an overall  $2.1 \pm 1.0 \text{ Tg yr}^{-1}$  emission increase during 2009.5–2014.5. This additional emission is  $\sim 1.5$  times the North America inventory estimate of  $1.6 \text{ Tg yr}^{-1}$  for 2007. Considering estimates of co-emitted NMHC yields an estimate for a yearly total NMHC emissions increase of  $1.2 \pm 0.8 \text{ Tg yr}^{-1}$  ( $5.9 \pm 4.0 \text{ Tg yr}^{-1}$  overall emissions increase during 2009.5–2014.5).



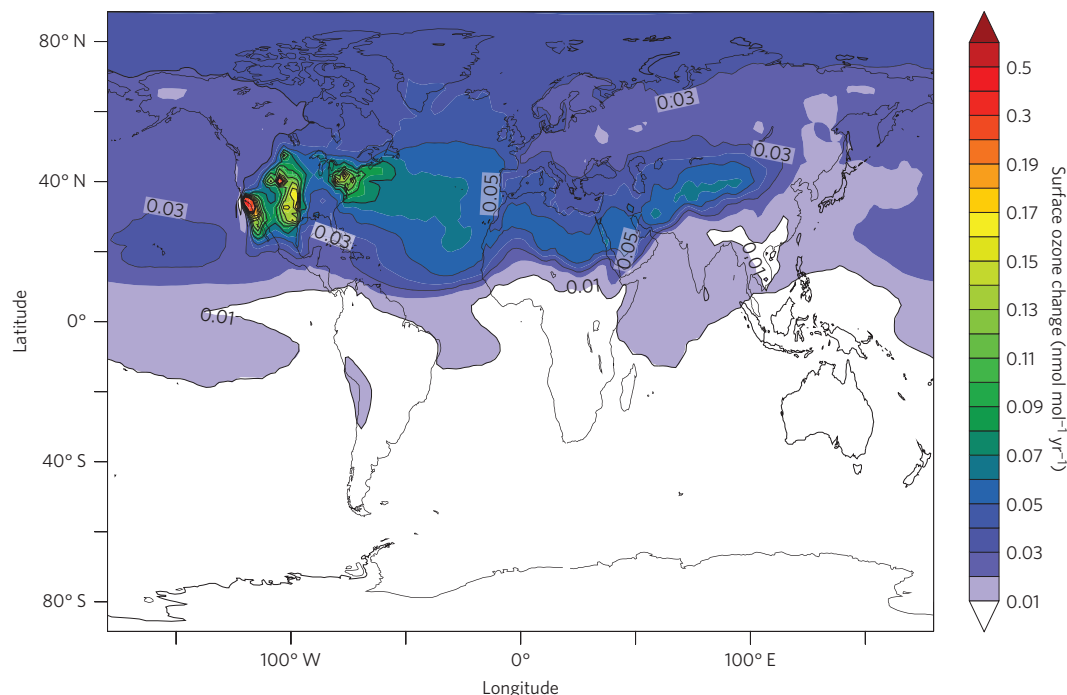


**Figure 4 | Ozone sensitivity study.** Estimate for the average annual 2009.5–2014.5 June–August change in surface ozone from a  $4.2\% \text{ yr}^{-1}$  NH increase in ethane, and inferred emission increases in propane, butane and pentane isomers from USA O&NG sources. The modelling did not consider increases in methane and NMHC  $>C_5$  emissions, and assumed constant emissions of nitrogen oxides and volatile organic compounds from other emission sectors. Increases in surface ozone are predicted over extended areas of the USA and downwind.

There is no evidence for major non-O&NG NMHC emissions increases. From the spatial overlap of USA O&NG regions with identified areas of largest NMHC increases it seems likely that the NMHC increase is largely driven by USA O&NG production. This added NMHC emission is expected to fuel additional surface ozone production in source and downwind regions. Figure 4 illustrates modelling results from a first order of magnitude sensitivity study, where the  $4.2\% \text{ yr}^{-1}$  increase in the  $C_2$ – $C_5$  NMHC flux was attributed to USA O&NG emissions over five years at constant emissions of nitrogen oxides ( $\text{NO}_x$ ). This added emission causes changes in surface ozone in regions with O&NG development and downwind, reaching up to  $0.5 \text{ nmol mol}^{-1} \text{ yr}^{-1}$  average ozone increases for June–August, corresponding to  $2.5 \text{ nmol mol}^{-1}$  increases overall over the five year period simulated with the model. The sensitivity is particularly high in the western USA, mostly driven by higher  $\text{NO}_x$  in that region. Consequently, these NMHC emission changes can potentially offset emission controls that have been implemented for curbing photochemical ozone production, and therefore can be a concern for attaining the ozone air quality standard.

Atmospheric methane has been increasing since  $\sim 2007$ , after a  $\sim 8$  year period of stable levels. Continental emission changes in methane are difficult to decipher because of the variety of biological, burning, and O&NG-related emissions, and the fact that trends are small relative changes in the large methane background. With shorter atmospheric lifetimes, trends of NMHC are more noticeable on a regional scale. Methane and ethane are co-emitted from O&NG sources in mass ratios of 1.7–33, with most results ranging from 7 to 14 (Supplementary Table 5). If we assume that the added ethane emission is entirely from O&NG sources, that the methane/ethane ratio from O&NG has not changed over time, and considering a median source region methane/ethane emission ratio of 10, an increase in the anthropogenic methane emission of  $4.4 \pm 3.1 \text{ Tg yr}^{-1}$  is estimated for the NH each year during 2009.5–2014.5. The cumulative increase in methane emissions implied from this approach would represent more than a doubling

of O&NG-related methane USA inventory emissions<sup>22</sup> and a  $\sim 6.2\%$  total increase between 2009.5 and 2014.5 of the  $330 \text{ Tg yr}^{-1}$  (ref. 23) global anthropogenic methane emission. Although other recent studies<sup>12,24–26</sup> have derived similar estimates for methane emission increases and associated those with increased North American O&NG emissions, most also rely on the extrapolation of NMHC results to infer methane emission changes. We note that surface and aircraft observations of methane stable isotopes from the GGGRN are inconsistent with such a large North American methane flux increase from O&NG sources<sup>27</sup>. Furthermore, the methane emission implied by this analysis of NMHC data as a fraction of O&NG production is a substantially higher percentage than what has been observed in O&NG fields in North America<sup>13,17,28–30</sup>. This suggests yet unidentified increasing sources for NMHC emissions independent of methane or with lower methane/ethane emission ratios, or potential emission increases outside North America that cannot be well defined at present owing to the sparsity of observations in those regions (for instance, in the Middle East, Africa, and Asia).

## Methods

Methods, including statements of data availability and any associated accession codes and references, are available in the [online version of this paper](#).

Received 12 November 2015; accepted 22 April 2016;  
published online 13 June 2016

## References

1. Aydin, M. *et al.* Recent decreases in fossil-fuel emissions of ethane and methane derived from firn air. *Nature* **476**, 198–201 (2011).
2. Worton, D. R. *et al.* Evidence from firn air for recent decreases in non-methane hydrocarbons and a 20th century increase in nitrogen oxides in the northern hemisphere. *Atmos. Environ.* **54**, 592–602 (2012).
3. Helmig, D. *et al.* Reconstruction of Northern Hemisphere 1950–2010 atmospheric non-methane hydrocarbons. *Atmos. Chem. Phys.* **14**, 1463–1483 (2014).

4. Nicewonger, M. R., Verhulst, K. R., Aydin, M. & Saltzman, E. S. Preindustrial atmospheric ethane levels inferred from polar ice cores: a constraint on the geologic sources of atmospheric ethane and methane. *Geophys. Res. Lett.* **43**, 214–221 (2015).
5. Von Schneidmesser, E., Monks, P. S. & Plass-Duelmer, C. Global comparison of VOC and CO observations in urban areas. *Atmos. Environ.* **44**, 5053–5064 (2010).
6. Warneke, C. *et al.* Multiyear trends in volatile organic compounds in Los Angeles, California: five decades of decreasing emissions. *J. Geophys. Res.* **117**, D00V17 (2012).
7. Simpson, I. J. *et al.* Long-term decline of global atmospheric ethane concentrations and implications for methane. *Nature* **488**, 490–494 (2012).
8. Kramer, L. J. *et al.* Seasonal variability of atmospheric nitrogen oxides and non-methane hydrocarbons at the GEOsummit station, Greenland. *Atmos. Chem. Phys.* **12**, 6827–6849 (2015).
9. Plass-Duelmer, C., Michl, K., Ruf, R. & Berresheim, H. C<sub>2</sub>–C<sub>8</sub> hydrocarbon measurement and quality control procedures at the Global Atmosphere Watch Observatory Hohenpeissenberg. *J. Chrom.* **953**, 175–197 (2002).
10. Read, K. A. *et al.* Intra-annual cycles of NMVOC in the tropical marine boundary layer and their use for interpreting seasonal variability in CO. *J. Geophys. Res.* **114**, D21303 (2009).
11. Leuchner, M. *et al.* Can positive matrix factorization help to understand patterns of organic trace gases at the continental Global Atmosphere Watch site Hohenpeissenberg? *Atmos. Chem. Phys.* **15**, 1221–1236 (2015).
12. Franco, B. *et al.* Retrieval of ethane from ground-based FTIR solar spectra using improved spectroscopy: recent burden increase above Jungfraujoch. *J. Quant. Spec. Radiat. Trans.* **160**, 36–49 (2015).
13. Pétron, G. *et al.* Hydrocarbon emissions characterization in the Colorado Front Range: a pilot study. *J. Geophys. Res.* **117**, 1–19 (2012).
14. Helmig, D. *et al.* Highly elevated atmospheric levels of volatile organic compounds in the Uintah Basin, Utah. *Environ. Sci. Technol.* **48**, 4707–4715 (2014).
15. Thompson, C. R., Hueber, J. & Helmig, D. Influence of oil and gas emissions on ambient atmospheric non-methane hydrocarbons in residential areas of Northeastern Colorado. *Elementa* **2**, 1–16 (2014).
16. Swarthout, R. F. *et al.* Impact of marcellus shale natural gas development in southwest Pennsylvania on volatile organic compound emissions and regional air quality. *Environ. Sci. Technol.* **49**, 3175–3184 (2015).
17. Karion, A. *et al.* Methane emissions estimate from airborne measurements over a western United States natural gas field. *Geophys. Res. Lett.* **40**, 4393–4397 (2013).
18. Schnell, R. C. *et al.* Rapid photochemical production of ozone at high concentrations in a rural site during winter. *Nature Geosci.* **2**, 120–122 (2009).
19. Oltmans, S. *et al.* Anatomy of wintertime ozone associated with oil and natural gas extraction activity in Wyoming and Utah. *Elementa* **2**, 1–15 (2014).
20. Vinciguerra, T. *et al.* Regional air quality impacts of hydraulic fracturing and shale natural gas activity: evidence from ambient VOC observations. *Atmos. Environ.* **110**, 144–150 (2015).
21. Schade, G. W. & Roest, G. S. Is the shale boom reversing progress in curbing ozone pollution? *EOS* **96**, <http://dx.doi.org/10.1029/2015EO028279> (2015).
22. *US Greenhouse Gas Inventory* (EPA, accessed 4 April, 2016); <https://www3.epa.gov/climatechange/ghgemissions/index.html>
23. Kirschke, S. *et al.* Three decades of global methane sources and sinks. *Nature Geosci.* **6**, 813–823 (2013).
24. Franco, B. *et al.* Evaluating ethane and methane emissions associated with the development of oil and natural gas extraction in North America. *Environ. Res. Lett.* **11**, 044010 (2016).
25. Hausmann, P., Sussmann, R. & Smale, D. Contribution of oil and natural gas production to renewed increase of atmospheric methane (2007–2014): top-down estimate from ethane and methane column observations. *Atmos. Chem. Phys.* **16**, 3227–3244 (2016).
26. Turner, A. J. *et al.* A large increase in US methane emissions over the past decade inferred from satellite data and surface observations. *Geophys. Res. Lett.* **43**, 2218–2224 (2016).
27. Schaefer, H. *et al.* A 21st century shift from fossil-fuel to biogenic methane emissions indicated by <sup>13</sup>CH<sub>4</sub>. *Science* <http://dx.doi.org/10.1126/science.aad2705> (2016).
28. Peischl, J. *et al.* Quantifying atmospheric methane emissions from the Haynesville, Fayetteville, and northeastern Marcellus shale gas production regions. *J. Geophys. Res.* **120**, 2119–2139 (2015).
29. Karion, A. *et al.* Aircraft-based estimate of total methane emissions from the Barnett Shale region. *Environ. Sci. Technol.* **49**, 8124–8131 (2015).
30. Petron, G. *et al.* A new look at methane and nonmethane hydrocarbon emissions from oil and natural gas operations in the Colorado Denver-Julesburg Basin. *J. Geophys. Res.* **119**, 6836–6852 (2014).

## Acknowledgements

This research would not have been possible without the contributions of many dedicated researchers that maintain the sampling programmes that provided the used data. The global VOC flask analyses are a component of NOAA's Cooperative USA- and global-scale Greenhouse Gas Reference flask sampling network, which is supported in part by NOAA Climate Program Office's AC4 Program. We greatly appreciate the work of many colleagues who have contributed to the programme operation and data processing, in particular C. Siso, P. Lang, J. Higgs, M. Crotwell, S. Wolter, D. Neff, J. Kofler, A. Andrews, B. Miller, D. Colegrove, C. Sweeney, E. Dlugokencky, and Y. Stenzel, and many unnamed CU Boulder undergraduate students who have processed the flask network data. The *in situ* monitoring at Summit is funded by the USA National Science Foundation, grant PLR-AON 1108391. We thank M. Fischer and S. Biraud for the operation of the STR and SGP site, respectively. The WGC and STR sites are operated with support from the California Energy Commission's Natural Gas programme under USA Department of Energy Contract No. DE-AC02-05CH11231. Financial support for the measurements at JFJ is provided by the International Foundation High Altitude Research Stations JFJ and Gornegrat (HFSJG), and for the GC/MS measurements also by the Swiss Federal Office for the Environment (FOEN) in the Swiss National Program HALCLIM. *In situ* VOC measurements at Cape Verde are made with the assistance of L. Mendes, K. Read, and J. Hopkins. The University of York thanks NCAS and NERC for funding. The FTIR measurements at NIWA, Lauder, are core funded through New Zealand's Ministry of Business, Innovation, and Employment. J.W.H. is supported by NASA under contract No. NNX13AH87G. The National Center for Atmospheric Research is supported by the USA National Science Foundation. The University of Liège contribution has been primarily supported by BELSPO and the F.R.S.—FNRS (Fonds de la Recherche Scientifique), both in Brussels. We thank P. Martinier, at LGGE, Grenoble, France, for the reconstructed ethane firm air history in Fig. 1a. The global VOC monitoring is under the auspices of the World Meteorological Organization Global Atmospheric Watch (WMO-GAW) programme, which facilitates coordination between participating partners and quality control efforts. The VOC World Calibration Centre is funded by the German Umweltbundesamt. We also thank the staff of the World Data Centre for Greenhouse Gases at the Japan Meteorological Agency for the archiving and public posting of data used in this study.

## Author contributions

D.H., study design, global flask network operation, Summit *in situ* measurements, data analyses, quality control, site comparisons, manuscript preparation. S.R., data processing, preparation of graphs, manuscript preparation. J.H., global flask network operation, analytical work, Summit *in situ* measurements. P.T., global flask network operation, manuscript preparation. S.A.M., propane data from the North American Tower flask programme and its quality control, manuscript preparation. K.M., NOAA network data management, NMHC global graphs shown in Fig. 2, manuscript preparation. K.T., data filtering, trend analyses, data statistics, manuscript preparation. C.P.-D., HPB NMHC monitoring, flask-*in situ* comparisons, manuscript preparation. A.C., HPB *in situ* NMHC monitoring. A.C.L., CVO NMHC *in situ* observations, manuscript preparation. L.J.C., CVO NMHC *in situ* observations, manuscript preparation. S.P., CVO NMHC *in situ* observations. S.R., JFJ NMHC *in situ* observations. M.K.V., JFJ NMHC *in situ* observations, manuscript preparation. R.S., VOC World Calibration Center, NMHC quality control, manuscript preparation. J.W.H., FTIR data evaluations and coordination, manuscript preparation. L.K.E., emissions modelling, ethane inventory data, manuscript preparation. E.M., JFJ FTIR data processing and analyses, manuscript preparation. B.F., JFJ FTIR data processing and analyses, manuscript preparation. D.S., Lauder FTIR observations and data processing, manuscript preparation. A.P., ethane inventory data, photochemical ozone modelling, manuscript preparation.

## Additional information

Supplementary information is available in the [online version of the paper](#). Reprints and permissions information is available online at [www.nature.com/reprints](http://www.nature.com/reprints). Correspondence and requests for materials should be addressed to D.H.

## Competing financial interests

The authors declare no competing financial interests.

## Methods

**Global VOC network.** Since 2004 the NOAA GMD and INSTAAR in Boulder, Colorado, have been operating a global volatile organic compound (VOC) monitoring programme that is building on the NOAA Global Greenhouse Gas Reference Network (GGGRN). VOCs are quantified in whole air sampled in pairs of glass flasks that are collected weekly to bi-weekly at ~44 global background monitoring sites, with a total sample number of ~3,000 per year. At present, ethane, acetylene, propane, *iso*-butane, *n*-butane, *iso*-pentane, *n*-pentane, isoprene, benzene, and toluene are analysed in the sample remaining in the flasks after completion of analyses of greenhouse gases, and of CO<sub>2</sub> and methane stable isotopic ratios. The gas chromatography (GC) with flame ionization detection method<sup>31</sup> is calibrated by a series of gravimetrically prepared synthetic and whole air standards. The programme operates under the umbrella of the World Meteorological Organization Global Atmospheric Watch (WMO-GAW) and is collaborating with international partners on exchange of calibration standards and comparison of calibration scales<sup>32</sup>. The INSTAAR laboratory was audited by the World Calibration Center (WCC) for VOC<sup>33</sup> in 2008 and 2011. Five unknown standards were analysed and results reported to the WCC. Mean results of five repeated measurements of the provided standards deviated <1.5% ethane, and <0.8% for propane from the certified values. These deviations are well below the deviation criteria set by GAW<sup>34</sup>. Uncertainties in the NMHC data are estimated to be ≤5% for results >100 pmol mol<sup>-1</sup>, and ≤5 pmol mol<sup>-1</sup> for results <100 pmol mol<sup>-1</sup>. More analytical and programme details are provided by refs 31,35,36.

**VOC *in situ* monitoring at Summit (SUM), Greenland.** Year-round VOC monitoring at Summit (72.6°N, 38.5°W; 3,216 m asl) was performed from 26 June 2008 to 22 July 2010, totalling 756 days (just over 2 years)<sup>37</sup>, and resumed in May 2012 and is ongoing. The GC is calibrated several times per week using standards that are cross-referenced against the global flask network laboratory scale. Uncertainties in the NMHC data are estimated to be ≤5% for results >100 pmol mol<sup>-1</sup>, and ≤5 pmol mol<sup>-1</sup> for results <100 pmol mol<sup>-1</sup>.

**VOC *in situ* monitoring at Hohenpeissenberg (HPB).** Continuous VOC monitoring at HPB (47.8°N, 11.8°E, 980 m asl) has been conducted since 1998 as part of the WMO-GAW<sup>9</sup>. Calibrations rely on a series of gravimetric and whole air standards referenced to the WCC. VOC sampling is conducted daily at noontime. Uncertainties (95% confidence interval) are generally ± (1.9 pmol mol<sup>-1</sup> + 2.9%) in the ethane mole fraction, and ± (1.3 pmol mol<sup>-1</sup> + 2.9%) for propane, except for isolated periods of degraded chromatography or other instrumental issues that result in higher uncertainties. Detection limits are at ~3 and 2 pmol mol<sup>-1</sup> for ethane and propane, respectively.

**VOC *in situ* monitoring at Jungfraujoch (JFJ).** At JFJ, a high-elevation site in the central Swiss Alps (46.5°N, 7.6°E, 3,580 m asl), VOCs are measured using a Medusa GC/mass spectrometer (MS)<sup>38</sup> hourly with each pair of measurements bracketed by standard measurements. Ethane and propane measurements started in 2008 and are ongoing. Measurement precisions are 0.3% for ethane and 0.8% for propane (1σ). Calibration is provided by referencing standards against primary reference gases of the National Physical Laboratories (UK) and thus is linked to the WMO-VOC scale. Uncertainties are ~10% for ethane and 3% for propane.

**VOC *in situ* monitoring at Cape Verde (CVO).** The Cape Verde Atmospheric Observatory Humberto Duarte Fonseca (16.8°N, 24.9°W, 10 m asl) is positioned upwind of Calhau on the northeastern side of São Vicente, Cape Verde. Hourly VOC measurements are made from a height of 20 m asl; analytical details are provided by ref. 10. Uncertainties in the NMHC data are estimated to be ≤5% for results >100 pmol mol<sup>-1</sup>, and ≤5 pmol mol<sup>-1</sup> for results <100 pmol mol<sup>-1</sup>. Detection limits are 2.6 and 1.6 pmol mol<sup>-1</sup> for ethane and propane, respectively. Calibrations are linked to the WMO-VOC scale.

**VOC measurements from North American tower sites.** Glass flasks are also collected with automated samplers at tower sites across North America as part of the NOAA GGGRN. These samples are collected at a higher sampling frequency (~daily) and are analysed at NOAA by GC/MS<sup>13</sup>. Reported mole fractions for propane are based on a suite of gravimetric standards prepared at NOAA; calibration consistency is maintained independently from INSTAAR. The resulting NOAA calibration scale for propane has been assessed in an international round-robin exercise and was found to be consistent within 5% to other internationally recognized and well-established scales<sup>39</sup>.

**Data processing.** At the time of the data processing final data from all considered sites until June 2014 (2014.5) were available, which was used as the cutoff of the analyses. The criterion for individual sites data to be included was that data were available for at least 50% of the sampling days for 2009.5–2014.5. Two flask network and three tower site data sets were excluded because they did not meet this

criterion. Similarly, *in situ* data from remote monitoring sites were only included if data were available for at least 50% of the 2009.5–2014.5 sampling dates.

NMHC data were first filtered for outliers; values that deviated more than 2σ from a running median were excluded from trend analyses. Filtered data were then uploaded to the NOAA server for filtering and trend determination using the method of ref. 40 and described at <http://www.esrl.noaa.gov/gmd/ccgg/mbll/crvfit/crvfit.html>. The first step is to fit a function, consisting of the sum of a polynomial and four harmonics (amplitude and phase of 1 through 4 cycles per year). The residuals of the function fit are smoothed by two low-pass filters, one for the trend (1.1 year full-width at half-maximum), and one for anomalies of the seasonal cycle (full-width at half-maximum 50 days). The function and filtered data are then combined to generate a smoothed data curve, trend curve, a detrended seasonal cycle, seasonal amplitude, a polynomial fit, and the long-term growth rate. The smoothed data curve is a combination of the function and the short-term filter of the residuals. The trend curve is the polynomial part of the function plus the long-term filtered residuals, and represents the growth or decline of the data with the seasonal oscillations removed. The detrended seasonal cycle is complementary to the trend curve; it is the interannually varying cycle with the trend removed. The seasonal amplitude is the amplitude of the detrended seasonal cycle, and the growth rate is the rate of increase or decrease of the trend, found by taking the first derivative of the trend. Results of a trends statistical significance test are included in Supplementary Tables 1 and 2. To avoid a bias from oversampling of the trend curve, its output was sampled only at times when retained flask data were available. These data were then subjected to the Mann–Kendall test<sup>41</sup> using a significance value of  $\alpha = 0.01$ . Results (calculated *p* values) are presented in column 12 of Supplementary Tables 1 and 2. Values <0.01 reflect the rejection of the null-hypothesis that there is no trend. In these cases, the trend is found to be true at 99% confidence. Incidences where trends were found to be not statistically significant are listed in italic font and in brackets. Results show that of 34 NH ethane trend series (flask and *in situ*), 32 show a positive trend. All positive trends are statistically significant. Lac La Biche, Alberta (LLB), shows a slight, nonsignificant negative trend. The LLB series has a reduced data coverage (73%), a high number of outlier points, and an  $R^2 = 0$  result, all of which reduce the robustness of the LLB trend result. The other site showing a negative trend is Black Sea, Constanta (BSC). Similar to LLB, this site suffers from reduced data coverage (50%), and a high number of outlier points. Furthermore, this site seems to be severely impacted by nearby pollution sources. Despite these two sites showing rather noisy records and poor regression results, they were retained in the presentation of our results, as we did not want to use arbitrary filtering criteria.

The data used in the maps (Fig. 3) were generated by applying a linear least-squares fit of the trend data from each site for the period 2009.5–2014.5. The slope of the fit determined the colour of the marker. The  $R^2$  value times the coverage of the fit determined the size of the marker. Most of the data are from NOAA/INSTAAR network flask sites. Furthermore, *in situ* monitored sites were included, as well as propane data from the tower sites.

Easter Island (EIC) propane data were excluded because they showed influence from a local source. Propane network data from BSC, and propane tower flask data from Mount Wilson Observatory (MWO) were excluded because a representative fit could not be drawn. A summary of trend results from all surface network and tower flask, and *in situ* observations is provided in Supplementary Table 1 for ethane, and in Supplementary Table 2 for propane.

**Network flask–*in situ* trend results evaluation.** There is overlap of flask and *in situ* VOC monitoring at two sites, that is, SUM and HPB. The parallel observations at these two sites were used to evaluate the quality of the trend fit results from the weekly network flask measurements against the higher time resolution *in situ* measurements. Details of these comparison studies will be presented in a forthcoming publication. In summary, these investigations showed that the less frequent flask records provide a good representation of the *in situ* records, yielding trend results of the same magnitude (Fig. 3).

**Average ethane trend calculations.** There are 45 sites that met the requirements (>50% data coverage for 2009.5–2014.5) for inclusion in the trend analyses, with 32 of these sites in the NH. As can be seen in Supplementary Tables 1 and 2, data coverage, quality of the correlation analyses, and trend results vary widely. We explored a number of methods for deriving an average NH ethane trend from these data. First, data from all sites, regardless of data coverage and quality of the regression fit, were treated equal. For sites with flask and *in situ* data, the mean of both trend values was used (SUM and HPB). Sites were grouped by latitude zone, NH longitude, and continental/oceanic region, and average and median ethane trends were calculated from all sites within each region (Supplementary Table 3). Please note the uneven representation of regions, as some of them have fewer sites than others, making results for regions with low representation less certain. Depending on the grouping and averaging, ethane trend results range from 3.5 to 4.3% yr<sup>-1</sup> for the mean values, and 2.9–4.2% yr<sup>-1</sup> for the median results across all sub-regions. The lower mean values are largely due to the negative trend



( $-7.6\% \text{ yr}^{-1}$ ) at BSC, a site that suffers from reduced data coverage (50%), and a high number of outliers, and seems to be severely impacted by nearby pollution sources (see above). Nonetheless, we kept the BSC result in the calculations for treating all sites equally for the NH mean trend calculations. Rates of increases are relatively high at Tiksi (TIK). Monitoring at TIK began in autumn 2011; therefore, the Tiksi record misses the first two years of the 2009.5–2014.5 window. The data coverage is just slightly above the 50% cutoff value (Supplementary Tables 1 and 2). TIK is the site with the second lowest coverage of all sites that were included. Given the short record the uncertainty is much higher than for other sites.

Second, a mean NH ethane trend was calculated by weighting each individual trend result (Supplementary Table 1) by the percentage of coverage of the data, and the  $R^2$  of the linear regression fit. For the two sites with flask and *in situ* measurements the mean value of both trends, a 100% coverage value, and the sum of both  $R^2$  values was used, to reflect the higher certainty from having two parallel results. The result of this analysis was a NH ethane increase rate of  $4.7\% \text{ yr}^{-1}$ . This value is relatively strongly influenced by the two highest individual results from two sites in the central USA, that is, Southern Great Plains (SGP) with a rate of change of  $10.7\% \text{ yr}^{-1}$ , and Park Falls (LEF), Wisconsin, with a value of  $7.9\% \text{ yr}^{-1}$ , also because both sites have full data coverage, and relatively high  $R^2$  results. Removing these two sites reduces the mean NH ethane rate of change to  $4.2\% \text{ yr}^{-1}$ . It is notable, though, that sites that are far distant from local influences, by horizontal separation, elevation, or by both, and located in the Atlantic region, downwind of North America, showed the cleanest records, that is, the highest correlation coefficient and on average relatively high rate of change values. Sites that fall into these categories (with their rate of change and  $R^2$  results) are SUM ( $63.9 \text{ pmol mol}^{-1} \text{ yr}^{-1}$ ,  $4.7\% \text{ yr}^{-1}$ ,  $R^2 = 0.97$  for flask results and  $67.2 \text{ pmol mol}^{-1} \text{ yr}^{-1}$ ,  $5.4\% \text{ yr}^{-1}$ ,  $R^2 = 0.96$  for *in situ*), Iceland (ICE) ( $46.2 \text{ pmol mol}^{-1} \text{ yr}^{-1}$ ,  $3.4\% \text{ yr}^{-1}$ ,  $R^2 = 0.86$ ), Mace Head (MHD) ( $53.1 \text{ pmol mol}^{-1} \text{ yr}^{-1}$ ,  $4.3\% \text{ yr}^{-1}$ ,  $R^2 = 0.65$ ), Azores (AZR) ( $86.7 \text{ pmol mol}^{-1} \text{ yr}^{-1}$ ,  $7.7\% \text{ yr}^{-1}$ ,  $R^2 = 0.57$ ), Assekrem (ASK) ( $72.9 \text{ pmol mol}^{-1} \text{ yr}^{-1}$ ,  $7.4\% \text{ yr}^{-1}$ ,  $R^2 = 0.95$ ), Tenerife (IZO) ( $30.0 \text{ pmol mol}^{-1} \text{ yr}^{-1}$ ,  $3.5\% \text{ yr}^{-1}$ ,  $R^2 = 0.32$ ) and CVO ( $44.7 \text{ pmol mol}^{-1} \text{ yr}^{-1}$ ,  $5.6\% \text{ yr}^{-1}$ ,  $R^2 = 0.96$ ). The mean weighted ethane rate of change from these North Atlantic sites accounts to  $5.3\% \text{ yr}^{-1}$ . These comparisons point towards highest rates of ethane increase in the central to eastern USA, followed by the North Atlantic region.

The overall hemispheric ethane trend result of  $4.7\% \text{ yr}^{-1}$  from the latter method using  $R^2 \times$  coverage as a weighting factor is  $0.4\text{--}1.8\% \text{ yr}^{-1}$  higher than the regional results presented in Supplementary Table 3. This possibly reflects a bias in the calculation as it places lower weight on sites with flat trends and corresponding low  $R^2$  results.

The uncertainty (0.9%) of the best estimate of the ethane NH rate of change was determined as 1/2 of the range of the lowest (2.9%) to the highest value (4.7%) of the different types of regional and hemispheric trend determination.

**NMHC surfaces.** Graphs in Fig. 2 were derived using weekly data from the GGGRN sites. To reduce noise in the latitudinal distribution due to synoptic-scale atmospheric variability, records were fitted with a smooth curve<sup>40</sup>. We then used a data extension methodology<sup>42</sup> with important revisions<sup>43</sup> to produce a set of smoothed records, which are synchronized in time and have no temporal gaps. For each synchronized weekly time step, a latitude distribution (mole fraction versus sine of latitude) was constructed. Each value in the weekly distribution was assigned a relative weight using a strategy that assigns greater significance to sites with high signal-to-noise and consistent sampling. A curve was then fitted to each weekly weighted latitudinal distribution<sup>44</sup>. Finally, values were extracted from each weekly latitudinal fit at intervals of 0.05 sine of latitude from  $90^\circ \text{ S}$  to  $90^\circ \text{ N}$  and joined together to create the two-dimensional matrix (time versus latitude) of mole fractions.

**FTIR column observations.** FTIR total and partial column data were derived from ongoing Network for the Detection of Atmospheric Composition Change (NDACC, [www.ndacc.org](http://www.ndacc.org)) observations from solar viewing FTIR instruments. The network instruments are calibrated to common standards to ensure consistent optical performance across the network and over time. High-resolution mid-infrared solar radiation is recorded on a near daily basis. Analyses of the JFJ ethane retrieval and time series are presented in ref. 12. An improved retrieval approach delivers enhanced information content and sensitivity up to  $\sim 20 \text{ km}$  altitude, providing two independent partial column time series, for the 3.58–8 and 8–21 km altitude. The ethane retrieval used for the Lauder spectra is presented in ref. 45. Initial analyses of Lauder time series are described in ref. 46, where SH decreasing trends are given up to 2009. The statistical bootstrap resampling tool used for the trend calculations is presented in ref. 47. It determines a linear trend and corresponding uncertainties, and accounts for the seasonal/intra-annual variability of the data. Determination of the uncertainty in the ethane column trend of the JFJ time series is explained in ref. 12. Several settings were tried (that is, adjusting the step and integration interval) for the running mean calculations at JFJ and other NH FTIR sites (for example, Toronto), always coming up with an ethane trend reversal date close to late 2008–early 2009.

**Emissions inventory.** The ethane emissions inventory is a best estimate based on three different resources that build on other previous inventories and publications. On the basis of reconstructed ambient air histories, a year 2000 global ethane emission was estimated at  $8\text{--}10 \text{ Tg yr}^{-1}$  (ref. 1). These authors do not differentiate between NH and SH emissions. Approximately 85% of ethane is estimated to be emitted in the NH (see (2) and (3) below). Based on that the global estimate translates to  $7\text{--}9 \text{ Tg yr}^{-1}$  of NH ethane emissions. Second, we evaluated the inventory developed for the Hemispheric Transport of Air Pollutants, Phase II (HTAP2), which is a composite of regional inventories harmonized to represent 2008 and 2010<sup>48</sup> emissions. Additional ethane emissions included in these simulations are biogenic emissions from the MEGAN2.1 (ref. 49), and fire emissions from FINNV1.5 (ref. 50). Simulations with CAM-chem indicated that the anthropogenic emissions needed to be doubled to match the pre-2009 NMHC FTIR observations at JFJ. A summary of these adjusted emissions by region and sources is given in Supplementary Table 4 for 2007. Year 2009.5 NH ethane emissions are estimated as  $15 \text{ Tg yr}^{-1}$  from the ‘Globe—all’ minus the SH emissions. For a third resource, we used the RCP85 database (Representative Concentration Pathway 8.5)<sup>51,52</sup>. It includes total emissions of ethane of  $\sim 12.9 \text{ Tg yr}^{-1}$ , of which 0.53, 2.3 and  $10 \text{ Tg yr}^{-1}$  are emitted from biogenic, biomass burning, and anthropogenic sources, respectively. Of the total  $12.9 \text{ Tg yr}^{-1}$ ,  $9.9 \text{ Tg yr}^{-1}$  are emitted in the NH.

We used  $9.9 \text{ Tg yr}^{-1}$ , which is the middle value of these three estimates for the ethane, NMHC, and methane emission increase, and ozone sensitivity modelling, and 1/2 of the minimum ( $7 \text{ Tg yr}^{-1}$ ) to maximum ( $15 \text{ Tg yr}^{-1}$ ) range as the uncertainty interval ( $4 \text{ Tg yr}^{-1}$ ).

**Scaling of methane to ethane.** The methane/ethane emission ratio was determined as the median of available data from analyses of both compounds in USA O&NG regions (Supplementary Table 5). We used 1/2 of the difference between the minimum and maximum value in the data as the uncertainty interval (5.6). The methane emission estimation uncertainty interval was calculated by error propagation including uncertainties in the ethane growth rate, the ethane inventory emission, and the methane/ethane ratio.

**Scaling of total NMHC to ethane calculation.** There are few publications that report speciated NMHCs, and there are even fewer that include ethane, from O&NG source regions. Furthermore, some of the available literature studies suffer from measurements being influenced to a variable degree by other contributing sources. We compiled published speciated NMHC/ethane emission ratios from O&NG development areas in Supplementary Table 6. Ambient air measurements were converted to relative mass emission ratios scaled to ethane. The contribution of missing NMHC to the total NMHC emission  $> \text{C}_2$  was estimated by adding up the relative fractions of missing species reported in the ref. 53 study and pro-rating the contribution of the missing species. There is a considerable amount of variability in these data, probably caused by the different NMHC emission ratios in different shale regions.

Among these data sets results from the Uintah Basin are likely to be of a relatively high representativeness for several reasons. First, despite the Uintah Basin having a low population density, atmospheric VOCs have been found to be highly elevated, dominated by emission from O&NG operations. In 2013 the basin had an estimated 4,300 oil- and 6,900 gas-producing wells; therefore, emissions reflect a combination of both types of wells. Second, this data set is the average over two campaigns from two subsequent years. Third, measurements represent an overall high number of samples. Fourth, data are from surface and tethered balloon measurements from January to February, when relatively shallow boundary layer conditions prevailed, which fostered accumulation of nearby emissions<sup>14</sup>.

The mean and median values for  $\Sigma \text{E}_{\text{NMHC}>\text{C}_2} / \text{E}_{\text{ethane}}$  from these studies were calculated as 2.47 and 1.85, respectively, with the Uintah Basin result being the medium value. For the reasons detailed above, we chose a Uintah median  $\Sigma \text{E}_{\text{NMHC}>\text{C}_2} / \text{E}_{\text{ethane}}$  value as scaling factor. The uncertainty of 1.4 was determined as 0.5 times the range of minimum to maximum scaling factors from individual studies. Uncertainty of the scaled total NMHC emission was calculated by error propagation.

**Ozone modelling.** EMAC (ECHAM5/MESy for atmospheric chemistry version 2.50<sup>54</sup>) was used to develop a first order of magnitude estimation of the impact of the emissions increase of simple NMHC on ozone formation. Although most of the added ethane flux is probably from the USA, other global regions may potentially have contributed to the flux increase. To reflect this uncertainty, we applied lower estimates for several of the applied variables. We did not consider an increase in methane emissions on ozone production. We considered only estimated associated emissions of  $\text{C}_2\text{--}\text{C}_5$ , excluding NMHC  $> \text{C}_5$ , which constitute  $\sim 10\%$  of the total O&NG NMHC emission (Supplementary Table 6), and on average have higher reactivity and ozone production potential than the lighter NMHC. Furthermore, the scaling value applied here is below the mean of available observations (Supplementary Table 6). The applied ethane NH inventory flux of  $9.9 \text{ Tg yr}^{-1}$  is a



significantly lower value compared with the most recent estimate ( $15 \text{ Tg yr}^{-1}$ , as explained above and in ref. 24). The model set-up was the same as in ref. 55, with the only exception of an augmented chemical scheme, which includes oxidation chemistry of simple  $\text{C}_4$ – $\text{C}_5$  hydrocarbons (that is, *n*- and *iso*-butane, and *n*- and *iso*-pentane). The model simulations adopted emissions from the RCP85 database (Representative Concentration Pathway 8.5)<sup>51,52</sup>. Two simulations were performed for 2009.5–2014.5: one with constant NMHC emissions, named CONST, and the other with increasing NMHC, named TREND. To disentangle the impact of increased NMHC emissions, all other tracer emissions were kept constant. We applied a trend of  $4.2\% \text{ yr}^{-1}$  for the NH emissions of ethane over five years based on the JFJ FTIR mid-troposphere column trend value. In the model NH emissions of ethane are  $\sim 9.9 \text{ Tg yr}^{-1}$ , of which 0.17, 0.9, and  $8.8 \text{ Tg yr}^{-1}$  are emitted from biogenic, biomass burning and anthropogenic sources, respectively. Therefore, the ethane growth rate accounts to an increase in ethane emission O&NG sources of  $\sim 0.41 \text{ Tg yr}^{-1}$ . Based on observed ambient air relative ratios of NMHC in source regions, see Supplementary Table 6, 0.30, 0.11, 0.08, 0.05 and  $0.06 \text{ Tg yr}^{-1}$  increases were prescribed to propane, *n*-butane, *iso*-butane, *n*-pentane, and *iso*-pentane, every year for five years, so that after five years the total emission increase was five times these listed emissions. Uncertainties in all scaling ratios propagate into the calculated ozone changes. The emissions map was based on shale O&NG wells distribution, available at <http://frack.skytruth.org>. Information used for generating this map is based on 'voluntary disclosure reports submitted by oil and gas drilling operators' and relies on locations of more than 15,000 wells. We assumed that all wells emit the same amounts of NMHC, neglecting difference in wells size and leakage rate. Finally, the distributed map of the wells was aggregated in a  $0.5 \times 0.5^\circ$  regular map, and emissions were scaled on the basis of the well number density in each grid cell. The resulting emissions map (see Supplementary Fig. 1) identifies regions that have experienced recent growth of O&NG development, with regions of large emission increases in the central and northeastern USA.

Modelling results in Fig. 4 show the differences in the ozone molar fraction between model results from the simulation CONST and TREND. Note that these results are based on constant emissions of other precursors, including those of nitrogen oxides ( $\text{NO}_x$ ). Decreasing trends of  $\text{NO}_x$  over the USA and of VOCs in urban areas have led to a general decrease of ozone in many urban regions. Omission of these effects will cause a high bias of the ozone changes that were calculated here. Consequently, these model results should be considered as preliminary results, providing an indication of the direction of ozone effects from added O&NG emissions, and taken as motivation for more in-depth modelling of the net effect resulting from these emission changes.

**Data availability.** The NMHC surface data used for this research are available at <http://www.esrl.noaa.gov/gmd/dv/data> and <http://ds.data.jma.go.jp/gmd/wdcgg>. The FTIR column observations can be retrieved from <ftp://ftp.cpc.ncep.noaa.gov/ndacc/station>.

## References

- Pollmann, J. *et al.* Sampling, storage, and analysis of  $\text{C}_2$ – $\text{C}_7$  non-methane hydrocarbons from the US National Oceanic and Atmospheric Administration Cooperative Air Sampling Network glass flasks. *J. Chromatogr. A* **1188**, 75–87 (2008).
- Helmig, D. *et al.* Volatile organic compounds in the global atmosphere. *Eos Trans. AGU* **90**, 513–514 (2009).
- World Calibration Centre for Volatile Organic Compounds (WCC-VOC) (Karlsruhe Institute of Technology, accessed 14 April 2016); <http://www.imk-ifu.kit.edu/wcc-voc>
- A WMO/GAW Expert Workshop on Global Long-Term Measurements of Volatile Organic Compounds (VOCs) Report No. 171 36 (WMO, 2007).
- Pollmann, J., Helmig, D., Hueber, J., Tanner, D. & Tans, P. P. Evaluation of solid adsorbent materials for cryogen-free trapping—gas chromatographic analysis of atmospheric  $\text{C}_2$ – $\text{C}_6$  non-methane hydrocarbons. *J. Chromatogr. A* **1134**, 1–15 (2006).
- Global Atmospheric VOC Monitoring Program (Atmospheric Research Laboratory, Institute of Arctic and Alpine Research, University of Colorado, accessed 31 March 2016); [http://instaar.colorado.edu/arl/Global\\_VOC.html](http://instaar.colorado.edu/arl/Global_VOC.html)
- Helmig, D., Stephens, C. R., Caramore, J. & Hueber, J. Seasonal behavior of non-methane hydrocarbons in the firm air at Summit, Greenland. *Atmos. Environ.* **85**, 234–246 (2014).
- Miller, B. R. *et al.* Medusa: a sample preconcentration and GC/MS detector system for *in situ* measurements of atmospheric trace halocarbons, hydrocarbons, and sulfur compounds. *Anal. Chem.* **80**, 1536–1545 (2008).
- Rhoderick, G. C. *et al.* International comparison of a hydrocarbon gas standard at the picomol per mol level. *Anal. Chem.* **86**, 2580–2589 (2014).
- Thoning, K. W., Tans, P. P. & Komhyr, W. D. Atmospheric carbon-dioxide at Mauna Loa observatory. 2. analysis of the NOAA GMCC data, 1974–1985. *J. Geophys. Res.* **94**, 8549–8565 (1989).
- Yue, S., Pilon, P. & Cavadias, G. Power of the Mann-Kendall and Spearman's rho tests for detecting monotonic trends in hydrological series. *J. Hydrol.* **259**, 254–271 (2002).
- Masarie, K. A. & Tans, P. P. Extension and integration of atmospheric carbon-dioxide data into a globally consistent measurement record. *J. Geophys. Res.* **100**, 11593–11610 (1995).
- GLOBALVIEW (NOAA Earth System Research Laboratory Global Monitoring Division, accessed 4 April 2016), <http://www.esrl.noaa.gov/gmd/ccgg/globalview>
- Tans, P. P., Conway, T. J. & Nakazawa, T. Latitudinal distribution of the sources and sinks of atmospheric carbon-dioxide derived from surface observations and an atmospheric transport model. *J. Geophys. Res.* **94**, 5151–5172 (1989).
- Rinsland, C. P. *et al.* Multiyear infrared solar spectroscopic measurements of HCN, CO,  $\text{C}_2\text{H}_6$ , and  $\text{C}_2\text{H}_2$  tropospheric columns above Lauder, New Zealand ( $45^\circ \text{S}$  latitude). *J. Geophys. Res.* **107**, ACH 1-1–ACH 1-12 (2002).
- Zeng, G. *et al.* Trends and variations in CO,  $\text{C}_2\text{H}_6$ , and HCN in the Southern Hemisphere point to the declining anthropogenic emissions of CO and  $\text{C}_2\text{H}_6$ . *Atmos. Chem. Phys.* **12**, 7543–7555 (2012).
- Gardiner, T. *et al.* Trend analysis of greenhouse gases over Europe measured by a network of ground-based remote FTIR instruments. *Atmos. Chem. Phys.* **8**, 6719–6727 (2008).
- Janssens-Maenhout, G. *et al.* HTAP\_v2: a mosaic of regional and global emission griddmaps for 2008 and 2010 to study hemispheric transport of air pollution. *Atmos. Chem. Phys.* **15**, 12867–12909 (2015).
- Guenther, A. B. *et al.* The Model of Emissions of Gases and Aerosols from Nature version 2.1 (MEGAN2.1): an extended and updated framework for modeling biogenic emissions. *Geosci. Model Dev.* **5**, 1471–1492 (2012).
- Wiedinmyer, C. *et al.* The Fire INventory from NCAR (FINN): a high resolution global model to estimate the emissions from open burning. *Geosci. Model Dev.* **4**, 625–641 (2011).
- Riahi, K., Grübler, A. & Nakicenovic, N. Scenarios of long-term socio-economic and environmental development under climate stabilization. *Technol. Forecast. Soc. Change* **74**, 887–935 (2007).
- Pozzer, A. *et al.* AOD trends during 2001–2010 from observations and model simulations. *Atmos. Chem. Phys.* **15**, 5521–5535 (2015).
- Swarthout, R. F., Russo, R. S., Zhou, Y., Hart, A. H. & Sive, B. C. Volatile organic compound distributions during the NACHTT campaign at the Boulder Atmospheric Observatory: influence of urban and natural gas sources. *J. Geophys. Res.* **118**, 10614–10637 (2013).
- Jöckel, P. *et al.* Development cycle 2 of the modular earth submodel system (MESSy2). *Geosci. Model Dev.* **3**, 717–752 (2010).
- Pozzer, A. *et al.* Observed and simulated global distribution and budget of atmospheric  $\text{C}_2$ – $\text{C}_5$  alkanes. *Atmos. Chem. Phys.* **10**, 4403–4422 (2010).